

MANTLE CONVECTION, PLATE TECTONICS, AND VOLCANISM ON HOT EXO-EARTHS

JOOST VAN SUMMEREN, CLINTON P. CONRAD, AND ERIC GAIDOS

Department of Geology and Geophysics, University of Hawai'i at Mānoa, Honolulu, HI 96822, USA; summeren@hawaii.edu

Received 2011 April 1; accepted 2011 June 7; published 2011 June 29

ABSTRACT

Recently discovered exoplanets on close-in orbits should have surface temperatures of hundreds to thousands of Kelvin. They are likely tidally locked and synchronously rotating around their parent stars and, if an atmosphere is absent, have surface temperature contrasts of many hundreds to thousands of Kelvin between permanent day and night sides. We investigated the effect of elevated surface temperature and strong surface temperature contrasts for Earth-mass planets on the (1) pattern of mantle convection, (2) tectonic regime, and (3) rate and distribution of partial melting, using numerical simulations of mantle convection with a composite viscous/pseudo-plastic rheology. Our simulations indicate that if a close-in rocky exoplanet lacks an atmosphere to redistribute heat, a $\gtrsim 400$ K surface temperature contrast can maintain an asymmetric degree 1 pattern of mantle convection in which the surface of the planet moves preferentially toward subduction zones on the cold night side. The planetary surface features a hemispheric dichotomy, with plate-like tectonics on the night side and a continuously evolving mobile lid on the day side with diffuse surface deformation and vigorous volcanism. If volcanic outgassing establishes an atmosphere and redistributes heat, plate tectonics is globally replaced by diffuse surface deformation and volcanism accelerates and becomes distributed more uniformly across the planetary surface.

Key words: planetary systems – planets and satellites: interiors – planets and satellites: surfaces – planets and satellites: tectonics

Online-only material: color figures

1. INTRODUCTION

Recent discoveries of exoplanets with Earth-like mass and radius (Mayor et al. 2009; Howard et al. 2010; Borucki et al. 2011) have intensified debate on how such planets compare to Earth in other respects. Due to observational bias, many of the discovered exoplanets inhabit short-period, close-in orbits and have effective temperatures exceeding many hundreds of Kelvin. For such planets, a likely outcome of dynamical evolution is tidal locking to their parent stars and, most probably, capture into a 1:1 spin-orbit resonance (Correia & Laskar 2010). Synchronous rotation causes asymmetric insolation and, in the absence of a substantial atmosphere, a strong (hundreds to thousands of Kelvin) temperature contrast between these planets' permanent day and night sides, as has been estimated for CoRoT-7b (Léger et al. 2009) and is plausible for Kepler-10b (Batalha et al. 2011).

Characterization of exoplanet surfaces is challenging and numerical simulations can help determine possible scenarios. Subsolidus convection is likely within the silicate mantles of rocky exoplanets but its vigor and surface expression depend on mantle temperature, composition, and rheology. Within the solar system, Earth is the only planet that currently exhibits plate tectonics which, on a geologic timescale, regulates volatile species in Earth's atmosphere via volcanic outgassing, silicate weathering, and subduction of precipitated carbonate (Walker et al. 1981). Venus is thought to experience infrequent global-scale resurfacing events, possibly the result of mantle-wide episodic overturn and associated with the formation of a dense greenhouse atmosphere, e.g., Solomon et al. (1999). Mars has experienced recent substantial volcanism although there is no evidence for recent crustal mobility, suggesting a stagnant lid regime with convective activity in the mantle interior below a static single-plate lithosphere, e.g., Spohn et al. (2001). Elevated surface temperatures can affect a planet's interior dynamics (Lenardic et al. 2008) and its surface properties,

as exemplified by insolation-driven variations of Mercury's lithospheric strength (Williams et al. 2011). Although there are no examples in our solar system, a hemispheric contrast in surface temperature may influence the interior dynamics and surface expression of exoplanets.

Here, we investigate the effect of elevated surface temperature and strong surface temperature contrasts for Earth-mass planets on (1) patterns of mantle convection, (2) tectonic regimes, and (3) the rate and distribution of partial melting (volcanism). For this purpose, we conducted numerical simulations of mantle convection with imposed surface temperatures.

2. DESCRIPTION OF NUMERICAL MODEL AND PARAMETERS

We investigated planetary mantle convection through numerical simulations of an incompressible fluid at infinite Prandtl number using the classical Boussinesq formulation. The associated conservation equations for mass, momentum, and energy are solved numerically using the finite element package CitComS-3.1.1 (Zhong et al. 2000). We investigated effective Rayleigh numbers $Ra_{\text{eff}} = \rho_0 g_0 \alpha_0 \Delta T h^3 / (\eta_{\text{eff}} \kappa_0)$ in the range $\sim 10^5 - 10^7$, where ρ_0 , g_0 , α_0 , and κ_0 are the respective reference values for density, gravitational acceleration, thermal expansivity, and thermal diffusivity, η_{eff} is the time-averaged mantle viscosity, ΔT is the temperature contrast across the mantle, and h is the mantle thickness. Bottom and internal heating both contribute to the heat budget. Internal radiogenic heat production is uniformly distributed across the mantle domain and constant in time in our models. The non-dimensional internal heat generation rate, defined as $\gamma = h^2 H_0 / (\kappa C_P \Delta T)$ (Glatzmaier 1988), is set to 11; this corresponds to a dimensional heating rate of $H_0 = 4 \times 10^{-12} \text{ W kg}^{-1}$, close to the present-day chondritic heating rate (Turcotte & Schubert 2002).

Our calculations ignore dissipation of tidal forces that can contribute to mantle heating and thermal runaway, depending on orbital eccentricity and type of resonance (Běhounková et al. 2011). However, without external perturbations, tidal dissipation renders orbital eccentricity insignificant on Myr–Gyr timescales and tidal effects can be neglected.

For the mantle domain, we employ an annulus (bi-section of a three-dimensional spherical domain) that is aligned with the orbital plane. All domain boundaries are free-slip and two side boundaries are imposed at the antistellar point. We adopt Earth’s outer radius ($r_S = 6371$ km) and mantle thickness ($h = 2891$ km), and allocate 257×65 nodal points in the lateral and radial directions, respectively, with gradual mesh refinement toward the top and bottom boundaries where temperature variations are generally greatest.

To permit plate-like behavior of the surface boundary layer, we adopt a composite viscous/pseudo-plastic rheology in our models, following Tackley (2000a; 2000b). Temperature-dependent viscosity η_v is described by an Arrhenius-type law:

$$\eta_v(T') = \eta_0 \exp \left[23.03 \left(\frac{1}{1+T'} - \frac{1}{2} \right) \right], \quad (1)$$

where the reference viscosity is $\eta_0 = 5 \times 10^{20}$ Pa s, and T' is the dimensionless mantle potential temperature that relates to the dimensional temperature, T , as $T' = (T - T_S)/\Delta T$, with $\Delta T = 2400$ K the potential temperature contrast across the mantle and T_S the surface potential temperature. Viscosity changes by five orders of magnitude over the considered temperature range ($T' \in [0, 1]$) and generates a lithosphere over a weaker mantle. Pseudo-plastic yielding concentrates strain and allows for lithospheric breakup in confined regions that mimic subduction zones and spreading centers (Tackley 2000a; Richards et al. 2001). In regions where the model stress exceeds an assigned yield stress, σ_y , a yield viscosity is calculated as $\eta_y = \sigma_y/2\epsilon_{II}$, where ϵ_{II} is the second invariant of the strain rate tensor. The composite rheology is described as $\eta = \min(\eta_v(T), \eta_y)$. We did not consider strain- or strain-rate-weakening (Christensen 1983), or time-dependent damage rheology (Bercovici 1996), which could further enhance plate-like behavior but would significantly complicate our analysis.

We assign distinct temperature conditions for three contrasting cases. In a first set (“cold” or C-models) we apply a uniform, time-constant surface temperature $T_S = 273$ K, comparable to Earth. A second set (“hot” or H-models) mimics close-in planets (i.e., orbital distance of $a = 0.13$ AU around a solar mass star) with efficient heat redistribution and a uniform surface temperature of $T_S = 759$ K. A third set (“asymmetric” or A-models) considers planets on a similar close-in orbit that lack heat redistribution. For these models, the surface temperature decreases sinusoidally from the hot substellar point ($T_{\text{subst}} = 1073$ K) to the terminus and is kept constant on the night side at $T_S = 273$ K. For all models, the core-mantle boundary (CMB) potential temperature is uniform and constant at $T_{\text{CMB}} = 2673$ K. Each simulation is run for several billion years (Gyr) of model time and we exclude the first 1 Gyr of initial transients to focus on statistically steady-state behavior.

To quantify tectonic regimes, we make use of two previously defined diagnostics (Tackley 2000a). First, to quantify the localization of surface strain rates, we define “plateness” as $P = 1 - (f_{80}/0.6)$, where f_{80} is the area fraction that encompasses 80% of the total surface strain rate. $P = 0$ corresponds to strain localization for isoviscous convection. Second, lid

mobility M is defined as the ratio of the root-mean-square (rms) surface flow velocity relative to the rms velocity of the entire mantle domain, $M = v_{\text{rms}}^{\text{surf}}/v_{\text{rms}}^{\text{whole}}$. Models with plate-like behavior are characterized by $M \approx 1\text{--}1.5$ and for stagnant lid convection $M \sim 0$. To allow faster calculations, we made use of the symmetry of the problem and determined tectonic regimes (Section 3) for models of 180° opening angle, with side boundaries at the substellar and antistellar points. For four representative models the time-averaged P and M values differ by only 6% and 9%, respectively, when comparing models of 180° and 360° .

Pressure-release partial melting is calculated following Raddick et al. (2002). We only consider melting in regions where convective flow is upward and where real (potential + adiabatic) temperatures exceed the mantle solidus temperature ($T_r > T_{\text{sol}}$). For T_{sol} we use a parameterization for dry mantle peridotite with a 1 bar value of $T_{\text{sol}}^0 = 1373$ K and $dT_{\text{sol}}/dz = 3.3$ K km $^{-1}$, in rough agreement with experimental measurements (e.g., Hirschmann 2000). In melting regions, the local melting rate, q_m , is calculated as $q_m(\vec{x}, t) = df/dt = (df/dz)u_z(\vec{x}, t)$, where f is the degree of melting and $u_z = dz/dt$ is the upward convective flow velocity. We use a constant value $df/dz = 0.18\%$ km $^{-1}$ for the adiabatic melt production per kilometer of upwelling (Phipps Morgan 2001). The local melting rate, q_m , is subsequently integrated over each melt column to give the surficial melt distribution. We limit melt production to a maximum depth of 50 km, which results in a time-averaged melt production for a nominal Earth model (C150) consistent with Earth’s present-day melt production of ~ 20 km 3 yr $^{-1}$ (McKenzie & Bickle 1988). Our choice of maximum depth affects the total melt production but has only a small influence on the comparison between models or on surficial distributions of melt. Because side boundaries promote vertical flow and unphysical concentration of melt at the substellar point, we calculate melting from models with a 360° opening angle.

3. TECTONIC REGIMES

C-models show a variety of convection regimes for a progressive increase of the yield stress values σ_y . At $\sigma_y \leq 50$ MPa, continuous yielding prevents the formation of stiff surface plates. Instead, a mobile lid style of convection, characterized by diffuse surface deformation, occurs (Figure 1(a), red curve). At $\sigma_y \sim 150$ MPa, surface deformation is approximately plate-like with stiff surface plates separated by narrow regions of concentrated deformation. Surface plates exhibit approximately piecewise constant velocities (Figure 1(a), green curve) and converge toward subduction-like downwellings while diverging at localized spreading centers (Figure 1(d)). A further increase of the yield stress produces a more time-dependent solution with alternating periods of surface mobility and stagnation. For sufficiently high yield stress (800 MPa), surface mobility diminishes and stagnant lid convection persists (Figure 1(a), blue curve). To further demonstrate tectonic regimes, we show plateness P and mobility M in Figure 2. For the C-models (Figure 2(a)), plateness increases to $P \sim 0.75$ with increasing yield stress at high mobility ($M \sim 1\text{--}1.5$) until the lid mobility rapidly decreases ($M \sim 0$) around $\sigma_y \sim 250$ MPa (and plateness becomes irrelevant).

For the H-models, coherent lithospheric plates do not develop because low viscosities near the warm ($T_S = 759$ K) surface promote viscous deformation and suppress pseudo-plastic yielding, consistent with the predictions of Lenardic et al. (2008). Surface velocities are greater and have a more diffuse distribution than

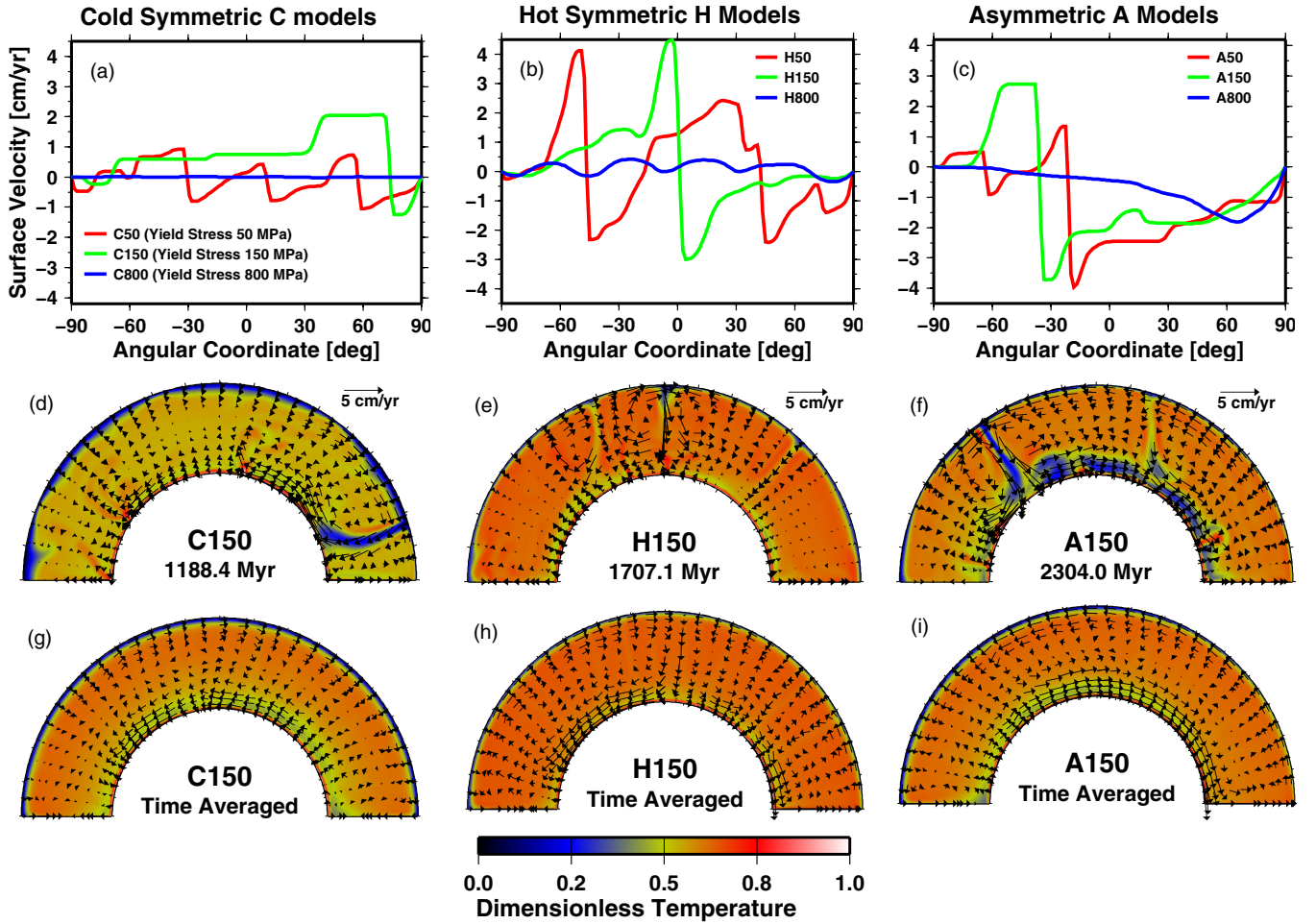


Figure 1. Top row: surface velocities for (a) cold symmetric C-models, (b) hot symmetric H-models, and (c) hot asymmetric A-models (see Section 2 for description). For all model types, three cases are shown with different yield stresses σ_y of 50 MPa (red curve), 150 MPa (green curve), and 800 MPa (blue curve). Middle row (d–f): snapshots of dimensionless potential temperature and convective flow velocity for models with $\sigma_y = 150$ MPa that correspond to the green curves in the top row. Bottom row (g–i): time-averaged values of the same quantities and models as in the middle row.

(A color version of this figure is available in the online journal.)

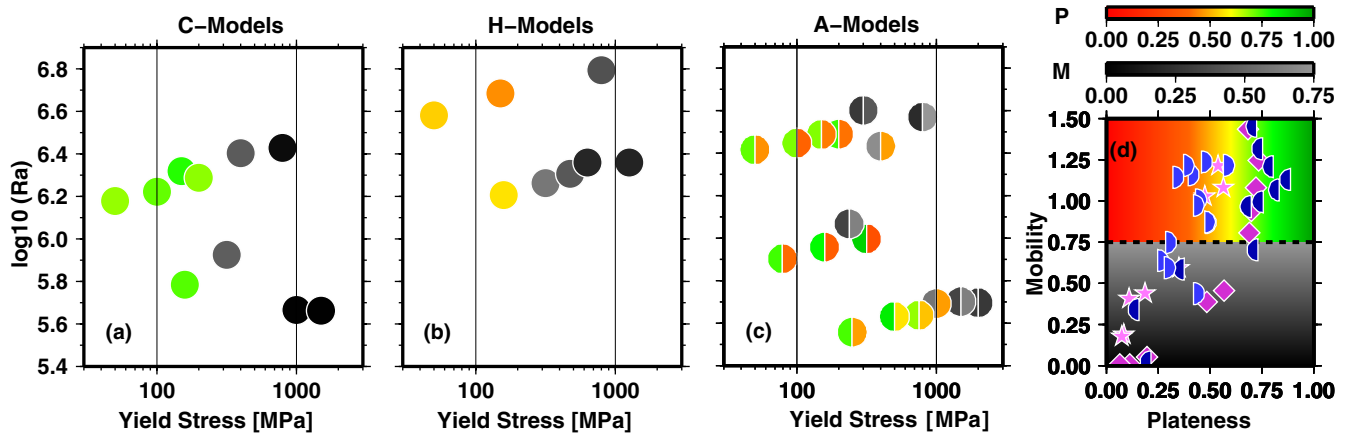


Figure 2. Diagnostics of tectonic regime (plateness, P , and mobility, M) for models with different Rayleigh number and yield stress. (a) “Cold symmetric” C-models, (b) “Hot symmetric” H-models, and (c) “Hot asymmetric” A-models, for which both day (right) and night (left) sides are shown. (d) All models in P – M domain space: C-models (dark purple diamonds), H-models (light purple stars), night side of A-models (dark blue left semi-circles), and day side of A-models (light blue right semi-circles). Color coding in (a–c) is for P -values if $M \geq 0.75$ and for M -values if $M < 0.75$, as indicated by the color bars above frame (d).

(A color version of this figure is available in the online journal.)

in the C-models (Figure 1(b)). Due to increased lithospheric mobility (e.g., model H150, Figure 1(e)) plateness is consistently lower for the H-models ($P \leq 0.5$, Figure 2(b)) compared

with the C-models ($P \sim 0.75$, Figure 2(a)). As σ_y increases, stagnant lid prevails but plate-like behavior is not observed (Figure 2(b)).

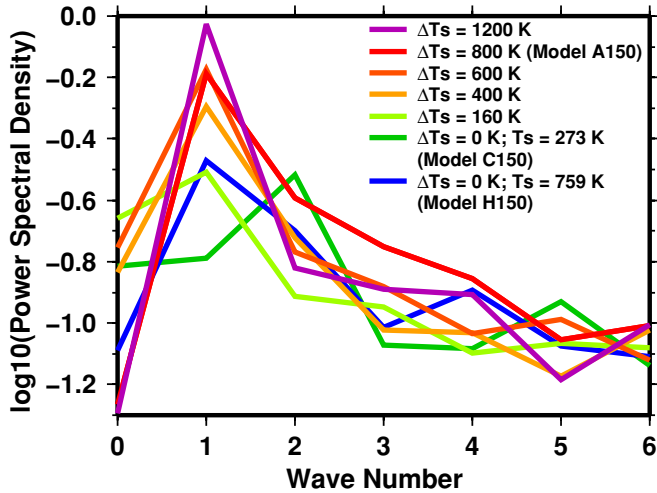


Figure 3. Power spectral density of time-averaged lateral convective flow velocity. Models with different surface temperature contrasts, ΔT_s , and surface temperatures, T_s , are compared.

(A color version of this figure is available in the online journal.)

For the A-models, a marked ($\Delta T_s = 800$ K) temperature contrast causes global-scale asymmetries in tectonic regime. Near the substellar point, high surface temperatures induce convective upwelling and diffuse surface velocities (Figures 1(c) and (f)). Away from the substellar point, plate-like behavior occurs and surface plates preferentially move toward the antistellar point (Figure 1(f)). A global scale dichotomy is reflected in the tectonic regimes diagnosed separately for the day and night sides (Figure 2(c)). The hot day side is consistently characterized by mobile lid convection with diffuse deformation, similar to the H-models (Figure 2(b)), while the cold night side exhibits plate-like behavior for a large parameter space, similar to the C-models (Figure 2(a)).

4. PATTERNS OF MANTLE CONVECTION

Flow patterns in the A-models are characterized by convective upwelling near the hot substellar point, near-surface flow from the hot day side to the cold night side where most downwellings occur, and a deep mantle return flow toward the day side (Figure 1(f)). An asymmetric degree 1 pattern of mantle flow persists, with convection cells that occupy the entire half-mantle domain (Figure 1(i)). For the C- and H-models with uniform surface temperature, convective downwellings are more randomly distributed across the domain and this results in less persistent convective flow (Figures 1(g) and (h)). As a diagnostic for persistent mantle flow, we use the rms value of the time-averaged flow velocity normalized by the time average of the rms flow velocities, or $\beta = (\overline{v})_{\text{rms}}/\overline{v_{\text{rms}}}$, where overlines indicate time-averaged values. The persistent flow in model A150 is reflected by relatively high time-averaged convective flow velocities ($\beta = 0.53$), compared to models with a uniform surface temperature, C150 ($\beta = 0.41$) and H150 ($\beta = 0.43$).

To estimate the surface temperature contrast ΔT_s that is required for maintaining asymmetric mantle flow, we compare power spectra of time-integrated lateral convective flow velocities for models with different ΔT_s (Figure 3). For surface temperature contrasts $\gtrsim 400$ K, a dominant degree 1 signal reflects persistent convection cells with upwelling at the substellar point and downwelling at the antistellar point. A systematic degree 1 signal is not discernible for models with $\Delta T_s < 400$ K and this

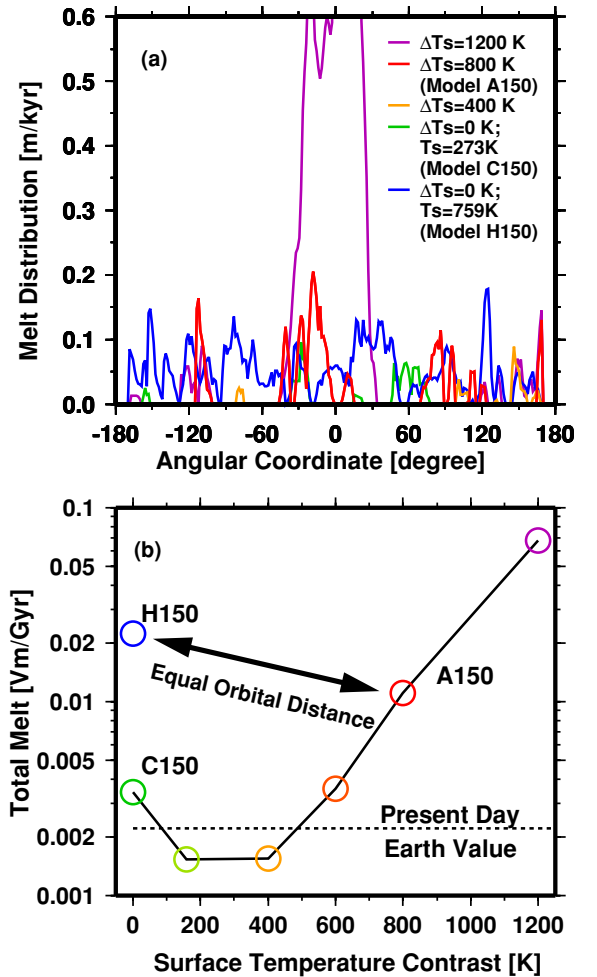


Figure 4. (a) Distributions of time-averaged melt production. Surface temperature contrasts, ΔT_s , and surface temperatures, T_s , for different models are color-coded as shown in the legend. The purple curve peaks at 1.18 m kyr^{-1} . (b) Total melt production, shown as a processing rate in mantle volume per billion years. The dashed line shows Earth's present-day melt production of $\sim 20 \text{ km}^3 \text{ yr}^{-1}$, corresponding to $\sim 0.002 \text{ V}_m \text{ Gyr}^{-1}$.

(A color version of this figure is available in the online journal.)

reflects more randomly oriented convection cells with a richer variety of length scales.

5. RATE AND DISTRIBUTION OF VOLCANISM

For surface temperature contrasts $\Delta T_s \lesssim 400$ K, melt rates show an uneven distribution without a coherent global pattern (Figure 4(a), green and orange curves) and a total melt production similar to the present-day Earth value of $\sim 20 \text{ km}^3 \text{ yr}^{-1}$ (McKenzie & Bickle 1988; Figure 4(b)). Above $\Delta T_s \sim 400$ K, melt occurs preferentially within upwellings near the hot substellar point (Figure 4(a), red and purple curves). Due to more persistent day side melting, the total melt production rises above the present-day Earth value by a factor of ~ 5 for $\Delta T_s = 800$ K and ~ 30 for $\Delta T_s = 1200$ K (Figure 4(b), red and purple circles, respectively).

For planets at the same orbital distance, more than double the amount of melt is produced in the model with uniform surface temperature H150 (Figure 4(b), blue circle) than in the asymmetric model A150 (Figure 4(b), red circle). Melting is more vigorous for model H150 because diffuse surface deformation occurs globally and is less vigorous for model A150

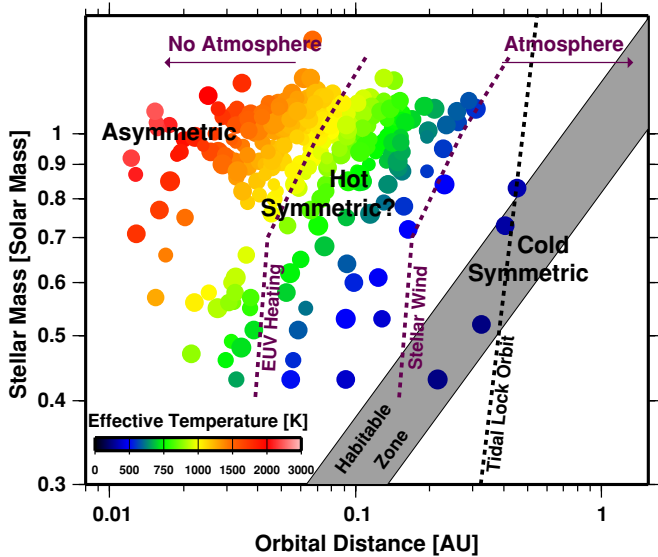


Figure 5. Possible occupation of planets in orbital distance–stellar-mass domain space. Purple dotted curves show atmospheric escape estimates for EUV heating for a $6 M_E$ planet (Tian 2009) and stellar wind erosion for an Earth-sized planet (Lammer et al. 2008). Tidal locking is likely at distances smaller than the tidal lock orbit (black dotted line; Kasting et al. 1993). Colored dots show effective temperatures, T_{eff} , for Kepler candidate exoplanets with $R < 2 R_E$ (Borucki et al. 2011). Different dot size reflects variability in planet size. For planets with a substantial atmosphere, uniform surface temperatures are expected. Planets without an atmosphere can have estimated substellar temperatures of $T_{\text{substellar}} \sim \sqrt{2}T_{\text{eff}}$ and a cold night side. The theoretical habitable zone lies between the 273 and 373 K isotherms where liquid water can be maintained.

(A color version of this figure is available in the online journal.)

because deformation occurs diffusely only near the substellar point.

6. DISCUSSION AND CONCLUDING REMARKS

Many recently discovered exoplanets inhabit close-in orbits and this results in high (hundreds to thousands of Kelvin) effective temperatures (Figure 5). Planets closer than 0.5 AU are likely to be tidally locked (Figure 5, black dotted line; Kasting et al. 1993) and synchronously rotating around their parent stars. At distances of < 0.1 AU, Earth-mass planets are unlikely to retain an atmosphere, due to atmospheric loss either by extreme ultraviolet (EUV) heating (Tian 2009) or stellar wind erosion (Lammer et al. 2008; Figure 5, purple dashed curves). These boundaries move outward for smaller planets that orbit around larger stars. The absence of a substantial atmosphere results in high substellar temperatures, approximated as $T_{\text{subst}} = \sqrt{2}T_{\text{eff}}$, and the night side remains cold. Thus, hot A-model behavior is expected for close-in orbits, and our results demonstrate that a persistent hemispheric surface temperature contrast $\gtrsim 400$ K can maintain a degree 1 pattern of mantle convection in which the planetary surface moves preferentially toward subduction zones on the cold night side. These planets should exhibit an inhospitable day side with vigorous volcanism and a cold night side that allows for more Earth-like tectonics and plate-like behavior. Melt production increases with increasing surface temperature contrast, and at 0.13 AU the calculated total melting rate is ~ 5 times higher than for a cool planet at 1 AU where plate tectonic behavior occurs globally (C-models).

At intermediate distances (~ 0.1 AU), an atmosphere is more likely to persist and atmospheric redistribution of heat is expected to produce a uniform hot surface. For such planets,

our H-model results demonstrate that mobility of the lithosphere prevents the formation of coherent plates and the emergence of Earth-like plate tectonics. Compared with an asymmetric model at the same orbital distance, melt production is enhanced by a factor > 2 and occurs globally across a surface that is characterized by diffuse deformation.

Our results suggest the possibility of different feedback mechanisms. Volcanic outgassing is responsible for the formation of secondary planetary atmospheres. Therefore, asymmetric conditions can only be sustained if the atmosphere is continuously eroded. If, instead, an atmosphere is retained, heat redistribution promotes mobile lid convection with diffuse deformation and further increases global volcanic outgassing. This suggests a positive feedback in favor of a thick atmosphere, unless another mechanism modifies the atmospheric balance. For example, no melt production is calculated for one-plate model planets, a possibility for potential close-in equivalents of present-day Venus. Atmospheres would be unprotected against solar wind erosion if a magnetodynamo is deactivated due to a transformation from plate tectonics to a regime that is less efficient at cooling the mantle and core (Buffett 2002; Christensen & Tilgner 2004; Gaidos et al. 2010). Substantial atmospheric loss would allow for a negative feedback and such planets could fluctuate between symmetric and asymmetric end-member scenarios or reach an intermediate equilibrium, depending on the timescale of atmospheric loss relative to mantle thermal evolution.

The dependence of tectonic regimes on σ_y for our nominal Earth models is consistent with previous studies performed using two-dimensional cartesian, three-dimensional cartesian, and three-dimensional spherical geometries (Moresi & Solomatov 1998; Tackley 2000a; Richards et al. 2001; Van Heck & Tackley 2008; Foley & Becker 2009). As in the above-mentioned studies, plate-like behavior occurs at yield stresses lower than classical estimates for dry oceanic lithospheric strength by up to ~ 1000 MPa (Kohlstedt et al. 1995), but weak fault zone fabric may account for this discrepancy (Moore & Rymer 2007; Escartin et al. 2008). The weak dependence of tectonic regimes on Ra shown in Figure 2(a) is in agreement with numerical results of Foley & Becker (2009) and scaling laws of plate tectonic convection by Korenaga (2010a, 2010b). Because a higher Ra is expected for more massive planets, this low sensitivity to Ra suggests that our results can be applied to planets of various sizes.

Convection in massive “super-Earth” mantles may be influenced by their more extreme pressure and temperature conditions. For example, mineral physics calculations suggest a viscosity decrease of 2–3 orders of magnitude for the deep mantles of super-Earths (Karato 2011), in favor of vigorous convective overturn. High mantle pressure allows for mineral phase transformations that do not occur in Earth’s mantle (Umemoto et al. 2006) but which can strongly influence the dynamics of super-Earth mantles (Van den Berg et al. 2010).

Although important questions remain, our simulations demonstrate the strong influence that surface temperature contrasts exert on mantle convection, surface tectonics, and volcanism for close-in rocky exoplanets. Distinct scenarios are likely associated with variations in albedo, volcanism, and atmospheric content that may become astronomically detectable in the future.

This research was supported by NSF grant EAR-0914712 and NASA grant NNX10AI90G. We thank Michael Manga, Edwin

Kite, Ray Pierrehumbert, and Maxim Ballmer for helpful discussions and an anonymous reviewer for constructive comments.

REFERENCES

- Batalha, N. M., et al. 2011, *ApJ*, **729**, 27
- Běhouňková, M., Tobie, G., Choblet, G., & Čadež, O. 2011, *ApJ*, **728**, 89
- Bercovici, D. 1996, *Earth Planet. Sci. Lett.*, **144**, 41
- Borucki, W.-J., et al. 2011, *ApJ*, **728**, 117
- Buffett, B. A. 2002, *Geophys. Res. Lett.*, **29**, 1566
- Christensen, U. 1983, *Earth Planet. Sci. Lett.*, **64**, 153
- Christensen, U. R., & Tilgner, A. 2004, *Nature*, **429**, 169
- Correia, A. C. M., & Laskar, J. 2010, in *Exoplanets*, ed. S. Seager (Tucson, AZ: Univ. Arizona Press), 526
- Escartin, J., Andreani, M., Hirth, G., & Evans, B. 2008, *Earth Planet. Sci. Lett.*, **268**, 463
- Foley, B. J., & Becker, T. W. 2009, *Geochem. Geophys. Geosyst.*, **10**, Q08001
- Gaidos, E., Conrad, C. P., Manga, M., & Hermlund, J. 2010, *ApJ*, **718**, 596
- Glatzmaier, G. A. 1988, *Geophys. Astrophys. Fluid Dyn.*, **43**, 223
- Hirschmann, M. M. 2000, *Geochem. Geophys. Geosyst.*, **1**, 2000GC000070
- Howard, A. W., et al. 2010, *Science*, **330**, 653
- Karato, S.-I. 2011, *Icarus*, **212**, 14
- Kasting, J. F., Whitmire, D. P., & Reynolds, R. T. 1993, *Icarus*, **101**, 108
- Kohlstedt, D. L., Evans, B., & Mackwell, S. J. 1995, *J. Geophys. Res.*, **100**, 17587
- Korenaga, J. 2010a, *J. Geophys. Res.*, **115**, B11405
- Korenaga, J. 2010b, *ApJ*, **725**, L43
- Lammer, H., Kasting, J. F., Chassefière, E., Johnson, R. E., Kulikov, Y. N., & Tian, F. 2008, *Space Sci. Rev.*, **139**, 399
- Léger, A., et al. 2009, *A&A*, **506**, 287
- Lenardic, A., Jellinek, A. M., & Moresi, L.-N. 2008, *Earth Planet. Sci. Lett.*, **271**, 34
- Mayor, M., et al. 2009, *A&A*, **507**, 487
- McKenzie, D., & Bickle, M. J. 1988, *J. Petrol.*, **29**, 625
- Moore, D. E., & Rymer, M. J. 2007, *Nature*, **448**, 795
- Moresi, L., & Solomatov, V. 1998, *GJI*, **133**, 669
- Phipps Morgan, J. 2001, *Geochem. Geophys. Geosyst.*, **2**, 2000GC000049
- Raddick, M. J., Parmentier, E. M., & Schreier, D. S. 2002, *J. Geophys. Res.*, **107**, 2228
- Richards, M. A., Yang, W.-S., Baumgardner, J. R., & Bunge, H.-P. 2001, *Geochem. Geophys. Geosyst.*, **2**, 2000GC000115
- Solomon, S. C., Bullock, M. A., & Grinspoon, D. H. 1999, *Science*, **286**, 87
- Spohn, T., et al. 2001, *Space Sci. Rev.*, **96**, 231
- Tackley, P. J. 2000a, *Geochem. Geophys. Geosyst.*, **1**, 2000GC000036
- Tackley, P. J. 2000b, *Geochem. Geophys. Geosyst.*, **1**, 2000GC000043
- Tian, F. 2009, *ApJ*, **703**, 905
- Turcotte, D. L., & Schubert, G. 2002, *Geodynamics* (2nd ed.; Cambridge: Cambridge Univ. Press)
- Umemoto, K., Wentzcovitch, R. M., & Allen, P. B. 2006, *Science*, **311**, 983
- Van den Berg, A. P., Yuen, D. A., Beebe, G. L., & Christiansen, M. D. 2010, *Phys. Earth Planet. Inter.*, **178**, 136
- Van Heck, H. J., & Tackley, P. J. 2008, *Geophys. Res. Lett.*, **35**, L19312
- Walker, J. C. G., Hays, P. B., & Kasting, J. F. 1981, *J. Geophys. Res.*, **86**, 9776
- Williams, J.-P., Ruiz, J., Rosenburg, M. A., Aharonson, O., & Philips, R. J. 2011, *J. Geophys. Res.*, **116**, E01008
- Zhong, S., Zuber, M. T., Moresi, L.N., & Gurnis, M. 2000, *J. Geophys. Res.*, **105**, 11063